Aquatic Ecosystem Health & Management
Publication details, including instructions for authors and subscription information:
http://www.tandfonline.com/loi/uaem20

Distribution and interannual variation of winter phytoplankton blooms northwest of Luzon Islands from satellite observations

Hui Zhao [a b c], Dandan Sui [a], Qiang Xie [a], Guoqi Han [c], Dongxiao Wang [a], Nancy Chen [c] & DanLing Tang [a]

[a] State Key Laboratory of Tropical Oceanography, South China Sea Institute of Oceanology, Chinese Academy of Sciences, Guangzhou, 510301, China

[b] South China Sea Environmental Institute, Guangdong Ocean University, Zhanjiang, 524088, China

[c] Fisheries and Oceans Canada, Northwest Atlantic Fisheries Centre, St. John's, NL, Canada

Published online: 20 Mar 2012.

To cite this article: Hui Zhao, Dandan Sui, Qiang Xie, Guoqi Han, Dongxiao Wang, Nancy Chen & DanLing Tang (2012) Distribution and interannual variation of winter phytoplankton blooms northwest of Luzon Islands from satellite observations, Aquatic Ecosystem Health & Management, 15:1, 53-61, DOI: 10.1080/14634988.2012.648875

To link to this article: http://dx.doi.org/10.1080/14634988.2012.648875

Distribution and interannual variation of winter phytoplankton blooms northwest of Luzon Islands from satellite observations

Hui Zhao,[1,2,3,*] Dandan Sui,[1] Qiang Xie,[1] Guoqi Han,[3] Dongxiao Wang,[1] Nancy Chen,[3] and DanLing Tang[1]

[1]*State Key Laboratory of Tropical Oceanography, South China Sea Institute of Oceanology, Chinese Academy of Sciences, Guangzhou 510301, China*

[2]*South China Sea Environmental Institute, Guangdong Ocean University, Zhanjiang 524088, China*

[3]*Fisheries and Oceans Canada, Northwest Atlantic Fisheries Centre, St. John's, NL, Canada*

[*]*Corresponding author: dxwang@scsio.ac.cn*

*Phytoplankton blooms often occur in the offshore region northwest of Luzon Islands in winter. Using remote sensing data, including sea-surface temperature, monthly-mean mixed layer depth (MLD), wind speed (SP), and SeaWiFS-derived chlorophyll-*a *(Chl-*a*) data from September 1997 to February 2007, we investigate the spatial and interannual variation of the winter phytoplankton in the region along with in situ GTS (the Global Telecommunications System) XBT (Expendable Bathythermograph) data and climatological nitrate and temperature observations from World Ocean Atlas 2005. The results clearly show high winter phytoplankton biomass (i.e. Chl-*a*) and its interannual variation in the region. The lower Chl-*a *concentrations (*$\sim$*0.2 mg m^{-3}) appeared often in winters (e.g. 1997 and 1998) when there was weaker wind speed, Ekman pumping velocity (EPV) and entrainment velocity (EV), and shallower MLD; conversely higher Chl-*a *(*$>$*0.5 mg m^{-3}) appeared in winters (e.g. 2001 and 2003) when there was higher subsurface temperature, stronger wind speed, EPV and EV, and deeper MLD. It is thought that wind-induced upwelling (Ekman pumping) and entrainment mixing may be important factors leading to the high winter Chl-*a*, and the wind speed and wind stress curl were good indicators of higher Chl-*a*; the positive correlation between subsurface temperature (and MLD) and Chl-*a *represented more warm water intrusion from the Northwest Pacific Ocean into the region in the higher Chl-*a *years.*

Keywords: Ekman pumping, entrainment, Northeastern South China Sea

Introduction

Marine phytoplankton biomass forms the basis of food chains in oceans and affects sea-surface CO_2 through photosynthesis, which contributes roughly half of the biosphere's net primary production (PP; Behrenfeld et al., 2006). An understanding of phytoplankton photosynthetic production and its role in carbon cycling has become increasingly fundamental to contemporary geosciences, and has been advanced tremendously by the application of ocean color remote sensing. Upwelling regions account only for 1% in the total area of the whole oceans, but the annual PP and the new PP in the upwelling regions are respectively 1.8% and 7.25% of the total PP for the whole oceans (Lalli and Parrsons,

Aquatic Ecosystem Health & Management, 15(1):53–61, 2012. ISSN: 1463-4988 print / 1539-4077 online
DOI: 10.1080/14634988.2012.648875

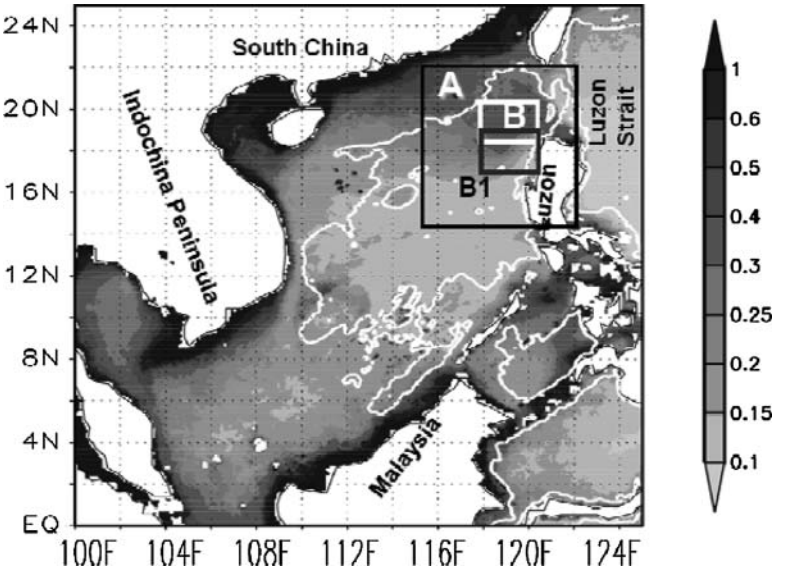

Figure 1. Winter chlorophyll-*a* (mg m^{-3}) climatology and location of the study area. Box A (15–23°N, 115–123°E): the study area, where the phytoplankton blooms often occur in winter; Box B (118–121°E, 18.5–20.5°N): a sampling area for satellite data; Box B1 (118–121°E, 17–19°N). The 2000 m isobath is also depicted (white contours).

1997). Due to the high output of phytoplankton and fishery, investigations of marine ecology in the upwelling regions have always been a hot topic for the last 50 years (Martin et al., 1987).

The South China Sea (SCS), with a total area of about 3.5×10^6 km^2, is the largest marginal sea in the western tropical Pacific Ocean (Figure 1). Luzon Strait, a channel between the Western Pacific Ocean and SCS, is about 350 km in width with a sill depth of about 1900 m. It is the most important channel for the exchange of the SCS deep water with the water of the open northwestern Pacific Ocean (Sverdrup et al., 1946). Previous investigations indicated that seasonal phytoplankton blooms and upwelling prevailed northeast of Luzon in winter (Gong et al., 1992; Liu et al., 1996; Shaw et al., 1996; Peñaflor et al., 2007). Pan et al. (2010) investigated the validation of satellite data in the northern SCS. The SCS is mostly controlled by oligotrophic water with abundant light year round (Liu et al., 2002; Zhao and Tang, 2007), and the mean annual PP is estimated to be only about 350 mg C m^2 d^{-1} (Liu et al., 2002). There are relatively low winter Chl-*a* contents (Figure 1) (<0.2 mg m^{-3}) in the deep basin with a depth over 2000 m; nevertheless high Chl-*a* content (>0.3 mg m^{-3}; Box B in Figure 1) appears evidently northwest of Luzon islands. Phytoplankton blooms in the region can exert an important influence on the SCS PP, fishery and the entire marine ecosystem. However, historical studies related to the blooms northwest of Luzon were based on only remote sensing observations for relatively short periods (Tang et al., 1999; Peñaflor et al., 2007) or sparse in-situ bio-hydrological measurements (Chen et al., 2006). Distribution and interannual variation of winter phytoplankton biomass west of Luzon were seldom investigated using longer terms of SeaWiFS Chl-*a* data, combined with other satellite and buoy's/historical observations.

In this paper, we emphasize interannual variation of the winter Chl-*a* bloom and influences of upper ocean conditions Northwest of Luzon, and probe into possible mechanisms underlying the winter phytoplankton bloom and its interannual variability.

Study Domain, Data and Methods

Study area and data sampling

Our study area lies in the northeastern SCS (Box A in Figure 1). In the area, the northeasterly monsoon appears in September, covering the entire SCS in November and generally reaching peak in December-January. The Kuroshio, a western boundary current of the North Pacific Ocean, and western tropical Pacific Ocean Water can interact

with the SCS through Luzon Strait (Shaw, 1991; Li et al., 1998). Intrusions of the Kuroshio as a loop into northeastern SCS and eddies shed from the Kuroshio into the SCS have been observed (Shaw et al., 1991; Li et al., 1998). The shape of intrusion circulation merged with distribution of wind stress curls and wind parallel to the coastline is favorable to induce upwelling in the region. In order to further expatiate quantitatively on the relationship between Chl-*a* and oceanic conditions (including surface winds), we chose a box, Box B1 (118 ∼ 121°E, 17 ∼ 19°N) in Figure1 for area-averaged time series, where the variations of wind speed, Ekman pumping velocity (EPV) and SST were more notable. Considering the lag time of phytoplankton growth for uptake of nutrients (the average turnover time being 2–6 days (Behrenfeld and Falkowski, 1997) and advections by the winter cyclonic circulation in the area (Hu et al., 2000; Morton et al., 2001), a patch of high Chl-*a* here may move northward in the east SCS. Thus, we chose Box B (118 ∼ 121°E, 18.5 ∼ 20.5°N) in Figure 1 as sampling areas for Chl-*a* and MLDs, which is equivalent to assume a northward current of 0.3 ∼ 1 m s^{-1}.

Data and Methods

SeaWiFS derived Chl-*a* data

Sea-viewing Wide Field-of-view Sensor (SeaWiFS) is operational since August 1997onboard the SeaStar spacecraft of NASA. In the present study, the Chl-*a* data are derived from SeaWiFS Version 4. Level 3 Monthly Standard Mapped Image (SMI) data were interpolated to a regular grid of equidistant cylindrical projection of 2160 × 4320 pixels (about 9.2 km), from October 1997 to July 2005. The data were obtained from the Distributed Active Archive Center (DAAC) of Goddard Space Flight Center (GSFC), NASA (http://oceancolor.gsfc.nasa.gov/cgi/level3.pl).

Sea Surface Temperature (SST), Mixed Layer Depths (MDL) and Sea Surface Wind

SST data from AVHRR Pathfinder Version 5 SST Project (spatial resolution 4 km with daytime) through Multi-Channel SST algorithm (McClain et al., 1985) and validation (Lee et al., 2005), which is a new reanalysis of AVHRR data stream, were obtained from Physical Oceanography Distributed Active Archive Center, JPL, NASA (http://podaac.jpl.nasa.gov/sst). The monthly-mean products for 1985–2007 are used in the present study.

Using their Thermal Ocean Prediction Model (TOPS) model, monthly-mean MLDs were calculated by the Fleet Numeric Meteorology and Oceanography Center (FNMOC) in Monterey, California and available from Oregon State University (http://www.science.oregonstate.edu).

Sea-surface wind speed (SP) and stress were obtained from the daily Quick Scatterometer (QuikSCAT) data provided by the Remote Sensing Systems in Santa Rosa, California (http://www.remss.com/). We also calculated the wind-induced Ekman pumping velocity (EPV) (Zhao and Tang, 2007). The entrainment velocity was estimated, based on EPV and MLDs according to Mendoza et al. (2005).

Hydrographic Data

The climatological profiles of in situ temperature, phosphate and nitrate of the World Ocean Atlas 2005 (WOA05) (Boyer et al., 2006) were imaged, and this was provided from the National Oceanographic Data Center (NODC) of NOAA (http://www.nodc.noaa.gov). The expendable bathythermograph (XBT) data of the Global Telecommunications System (GTS) were available from http://www.aoml.noaa.gov. Five sets of XBT data in Januaries of 2001–2005 are chosen at stations roughly inside Box B (i.e. 118–120°E 20–21°N). Vertical profiles of temperature were used to analyze the influence of vertical thermal structure on phytoplankton biomass.

Methods

By using the above-mentioned data of Chl-*a*, SST, SSW, EPV, EV and profiles of climatological temperature, phosphate and nitrate, monthly-mean climatology during the winter season (November–March) was produced for a period as long as these data are available. For further evaluating changes of the Chl-*a*, time series of Chl-*a* and MLD were constructed by averaging them over Box B in Figure 1. The SST, EPV, EV, and SP were averaged over Box B1 (Figure 1) to probe into the mechanism of winter high Chl-*a*.

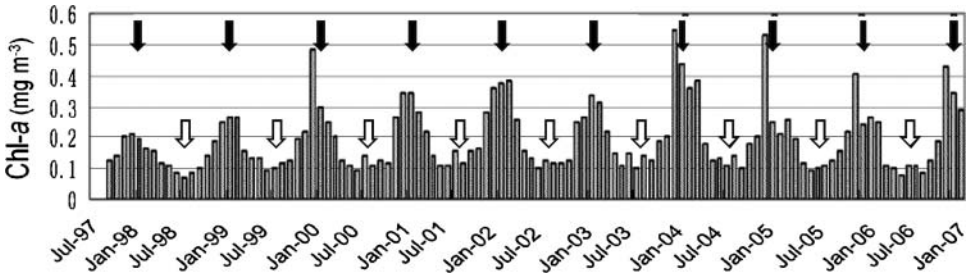

Figure 2. The time series of Chl-*a* concentrations averaged for Box B (Figure 1). X-axis represents yearly dates (month). Solid and open arrows point to January and July from 1998–2007, respectively.

Results

Winter high Chl-*a* concentration northwest of Luzon and temperature profiles

As shown in the climatology of Chl-*a* averaged for winter (Figure 1), the low Chl-*a* (<0.15 mg m^{-3}) was only observed in the western Pacific Ocean and offshore regions south of 20°N. The patch of high Chl-*a* (>0.3 mg m^{-3}) in winter covering Box B in Figure 1 and Figure 2 appeared evidently northwest of Luzon. The climatology for winter months (Figure 3, A1–A3) showed also obviously high Chl-*a* concentration (>0.3 mg m^{-3}) roughly in the similar location.

The time series (Figure 2) of Chl-*a* concentrations averaged for Box B (B in Figure 1) represents the monthly variation of Chl-*a* during September 1997 to February 2007 and shows high concentrations (>0.2 mg m^{-3}) up to 0.5 mg m^{-3} in winter and low concentration (<0.1 mg m^{-3}) in summer. The maximum of monthly Chl-*a* concentrations typically occurred in December/January in almost every winter (solid downward arrows in Figure 2), confirming annual recurrence of winter phytoplankton blooms in the region. The Chl-*a* showed evident interannual variability with the highest peak of 0.55 mg m^{-3} in December 2003 and the lowest value of 0.21 mg m^{-3} in December 1997.

Levitus temperature and nitrate concentration

Due to cooling and strong mixing induced by strong winter monsoon, it is likely difficult to distinguish upwelling tendency from mixing effects. Here, we used the temperature at the depth of 75 m ($Temp_{75}$) as the indicator for upwelling. The $Temp_{75}$ climatology (Figure 3b) for winter displayed obviously a low temperature patch (<21°C) northwest of Luzon; however, warm temperature is prevalent northeast of Luzon (>23°C) and in the surrounding area (>22°C). The low temperature patch (Figure 3 b1–3) in winter may indicate that upwelling tendency was prevalent northwest of Luzon in these winter months. Though the spatial resolution of the monthly nitrate concentration from Levitus is low ($1° \times 1°$), the winter climatology of nitrate concentration averaged for the upper 75 m (Figure 3c) displayed a patch of high nitrate concentration (>2.5 μg m^{-3}) in roughly the similar location with the low $Temp_{75}$ patch northwest of Luzon, which supports the existence of upwelling in the region northwest of Luzon.

MLD northwest of Luzon in winter

In winter, MLDs deepen generally due to vigorous mixing induced by strong winter monsoon and cooling tendency for upper oceans resulted from heat losses and southward advection of cold water in northern SCS. Thus, deep MLD (>60 m; Figure 3D) appeared in the western Pacific Ocean and offshore regions south of China. Nevertheless, shallow MLDs were observed northwest of Luzon, approximately near the high Chl-*a* patch (Figure 3a) and the low $Temp_{75}$ patch (Figure 3b), as well as the high nitrate patch (Figure 4c).

Wind speed and EPV in winter

The wind vectors and EPV patterns (Figure 3E) presented strong northeasterly winds (>10 m s^{-1}) and downwelling tendency ($<-1 \times 10^{-6}$ m s^{-1}) implied by negative EPV in most of the northeast SCS. Nevertheless, strong upwelling tendency from EPV ($>1 \times 10^{-5}$ m s^{-1}; Figure 3e) can be observed northwest of Luzon, located in 118°–120°E and 17°–19°N (Figure 3e) roughly similar to the location of the low $Temp_{75}$ patch. Results showed also

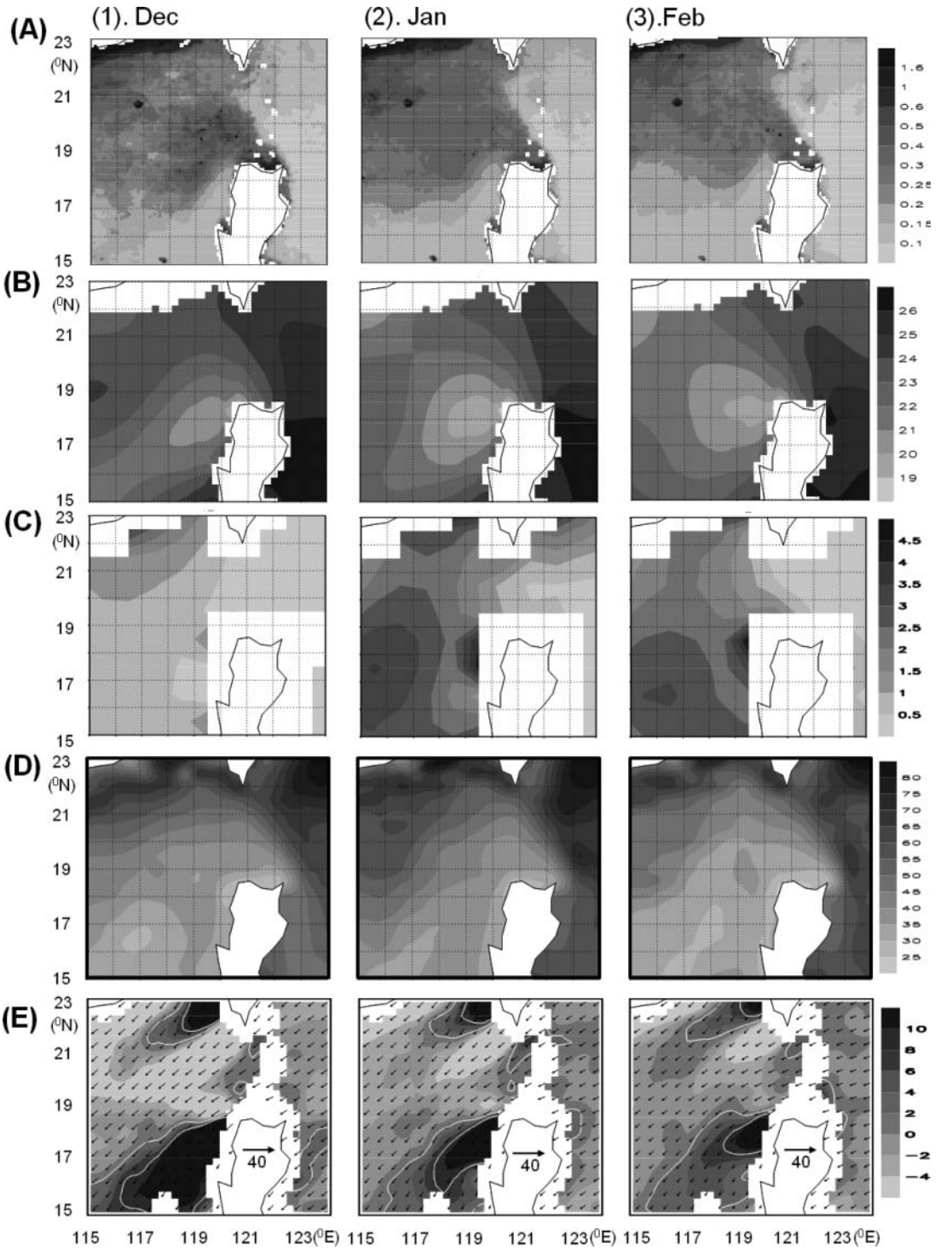

Figure 3. The climatologies averaged for winter months. (a) Chl-*a* from 1997–2006 (mg m^{-3}); (b) Levitus Temperature (°C) and (c) Nitrate (ug m^{-3}) at 75 m depth; (d) Mixed Layer Depth (m) from 1997–2006; (E) Ekman Pumping Velocity (shaded, in 10^{-6} m s^{-1}) and Surface Wind Speed (arrow vectors, in m s^{-1}).

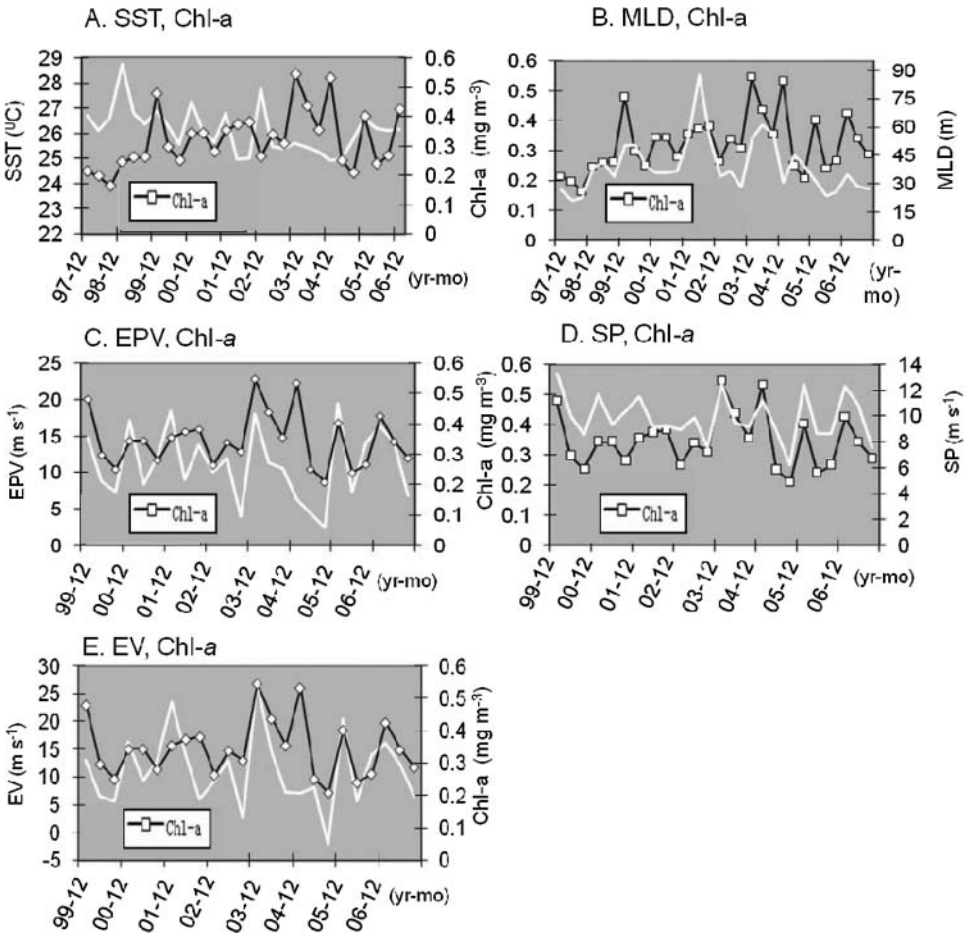

Figure 4. Time series data sampled from Box B and Box B1 in Figure 1 for the winter period of 1997–2007 (a–b) and 1999–2007 (c–e) Sea Surface Temperature (SST); Chl-*a* (mg m^{-3}); Mixed Layer Depth (MLD) (m); Ekman Pumping Velocity (10^{-6} m s^{-1}), (EPV); Surface Wind Speed (SP) (m s^{-1}); Entrainment velocity, (10^{-6} m s^{-1}) (EV).

that the region of this strong EPV occurred generally in the same locations south of the region of high Chl-*a* patch during December–February.

Time series of Chl-*a*, SST, MLD, EPV, SP and EV in winter

Time series of monthly Chl-*a*, SST, MLD, EPV, SP and EV (Figure 4) for winter months (December-February) was produced for Box B1 and B (Figure 1) northwest of Luzon. The time series showed evident interannual variability of Chl-*a*, SST and MLD. The relationship between Chl-*a* and SST is not significant, with a negative correlation coefficient (Correlation coefficient: $R = -0.297$; Level of significance: $P > 0.05$). In contrast, Chl-*a* presented significant correlation with MLD ($R = 0.445$, $P < 0.05$). There was also significant positive correlation (Figure 4c–4e) between Chl-*a* and EPV ($R = 0.5$), SP ($R = 0.74$) as well as EV ($R = 0.70$) at the level of significance of 0.01.

Chl-*a* and XBT vertical temperature in winter

Here, we selected a set of XBT temperature data inside Box B (Figure 1) in January from 2001–2005 as a proxy of the winter water temperature. The XBT profiles in the upper 100-m depth (Figure 5a) indicated high mean temperature in January of 2002 and 2004 and low mean temperature in January of 2001 and 2003, highest in 2004 and lowest in 2003. According to the time series of the temperature at the depth of 75 m ($Temp_{75}$) and the Chl-*a*

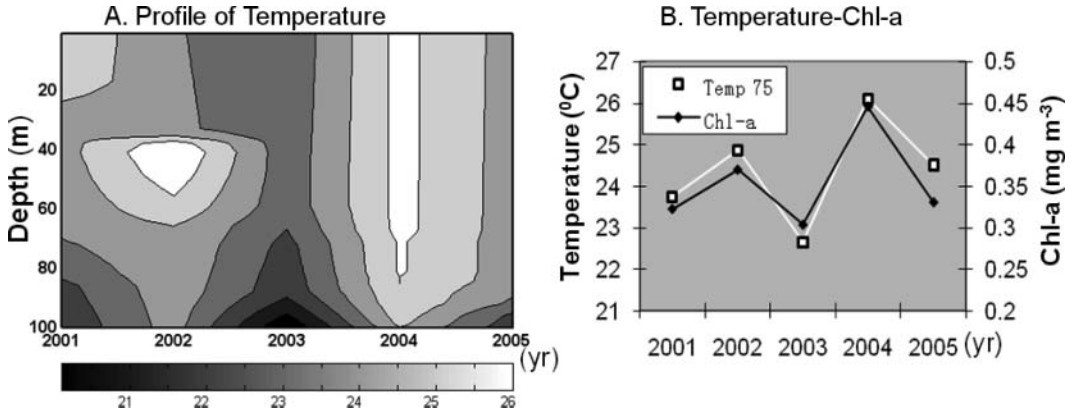

Figure 5. (a) Profile of temperature (°C) and (b) time series of temperature at 75-m depth (°C) and Chl-*a* (mg m^{-3}) for January from 2001–2005 in Box B (Figure 1).

concentration averaged for winter (December-January) (Figure 5B), the $Temp_{75}$ and Chl-*a* presented also a good positive correlation ($R = 0.929$, $P < 0.05$), i.e. high Chl-*a* vs. high temperature.

Discussion

The winter high Chl-*a* patch

Nutrients such as nitrate and phosphate are limiting factors for marine phytoplankton in tropical oceans. In upper tropical oceans with abundant sunlight, nutrients are generally low in a photic layer (Levitus et al., 1994) because of consumption by phytoplankton and block of injection of nutrient into the upper layer by the pycnocline. Ocean water temperature is generally lower below the upper mixed layer. Thus, horizontal pattern of temperature or SST is usually taken as an important indicator for upwelling, which can entrain nutrients into the euphotic zone as well as phytoplankton closer to the surface so that their photosynthetic system receives greater solar irradiance.

In the present study, according to the vertical profiles of Levitus climatology of temperature and nitrate (Figures 3b–3c), the significant upwelling tendency and increasing concentration of nutrients (i.e. nitrate concentration) were verified in the region northwest of Luzon, consistent with Tang et al. (1999) and Wang et al. (2003). In regions of strong wind, mixing entrainments may lead to deepening of MLD, increasing nutrient-rich water into upper oceans and triggering higher Chl-*a* concentration, in turn. On the other hand, in upwelling regions, upwelling tendency can generally induce uptake of sub-surface water and divergence of sea surface water, reducing the MLD. Thus, as shown in Figure 3d, shallower MLD implies higher Chl-*a* in regions dominated by wind-induced upwelling. It is a possible reason leading to higher phytoplankton in winter than that in other seasons (Figures 1 and 2). Moreover, coinciding roughly with the region of high Chl-*a,* the ocean data along 18.5°N displayed respectively shallower MLD, stronger EPV and wind speed in the region, compared with regions in the western Pacific Ocean or the SCS close to the region, respectively (Figures 3d and 3e), indicating possible prevailing upwelling tendency in the region. Winter upwelling tendency northwest of Luzon was also validated in the region using ocean models/observational data (Gong et al., 1992; Liu et al., 1996; Shaw et al., 1996), consistent with our study. At the same time, high phytoplankton biomass in winter was also reported in previous studies (Tang et al., 1999; Peñaflor et al., 2007). Therefore we conjectured that the patch of high Chl-*a* observed northwest of Luzon may be mainly triggered by increasing nutrient level through enhanced EPV associated with the wind stress curl and strong entrainment mixing associated with strong wind and heat loss (Figures 3 and 4). Note that the maximum Chl-*a* often occurred in December instead of January, which may be attributed to the influence of zooplankton growth time lagging (Chen et al., 2006; Olivieri, 1983), leading to high grazing pressure in January.

In addition, fronts/eddies due to the intrusion of the Kuroshio and the northward movement of the northward coastal current west of Luzon (NCCWL) may also exert certain influence on the

winter phytoplankton blooms (Chao et al., 1996; Shaw et al., 1996; Fang et al., 1998).

The interannual variation of the winter high Chl-*a* patch

The winter Chl-*a*, SST, EPV, SP and MLD in Figure 4 all clearly displayed interannual variation in the region northwest of Luzon. Nutrients (temperature) are generally higher (lower) at deeper layers according to Levitus climatology (Boyer et al., 2006). Thus, upwelling and mixing entrainment can influence abundance of nutrients available to phytoplankton, elevating Chl-*a* concentration. Compared with surrounding water column, upwelling tendency may lead to shoaling of the MLDs and doming of isotherms and divergence of sea surface water (Udarbe-Walker and Villanoy, 2001). Thus, interannual changes in MLDs and vertical temperature might reflect variation of upwelling intensity.

Previous studies showed considerable upwelling northwest of Luzon, attributable to positive wind stress curl (Qu, 2000), to subsurface convergence of the NCCWL during NE monsoon (Chao et al., 1996; Shaw et al., 1996), or to cyclonic eddies (Hu et al., 2000; Wang et al., 2003; Han and Huang, 2009). As shown in Figure 3, vertical and horizontal conditions of the region affirmed also prevalent upwelling in the region in winter.

The present study indicated EPV and EV are significantly correlated with Chl-*a* concentration, implying that the phytoplankton blooms were mainly triggered by the nutrient enhancement through wind-induced upwelling and through vertical entrainment due to wind forcing and heat loss. The interannual variation of the winter SST and MLD is more complicated. Farris and Wimbush (1996) displayed that stronger northeast monsoon can trigger intrusion of the Kuroshio Current and stronger cyclonic current loops into Luzon Straits. The Kuroshio Current from the Northwest Pacific has higher temperature and MLD (Figure 3). Higher temperature of the intruding Kuroshio water works against the effect of the surface wind mixing and heat loss as well as the subsurface upwelling on SST. This may be the reason that the SST cannot reflect upwelling in the present study. The positive correlation between the winter MLD and Chl-*a* is somewhat unexpected. A plausible explanation is that although the upwelling generally reduces the MLD as discussed in 4.1, the far deeper MLD of the intruding Kuroshio water could overcome the upwelling effect completely. Indeed, the high positive correlation between Chl-*a* and the $Temp_{75}$ in the region (Figure 5b) suggests that the intrusion of warm water from the Northwest Pacific Ocean was stronger during these years with higher Chl-*a,* EV and EPV, as shown in Figures 4–5.

Moreover, Kuroshio Current loops and the fronts due to the intrusion of the Kuroshio and northward current along the west Luzon coastline can also be important for nutrients transport or advection (Farris and Wimbush, 1996; Hu et al., 2000; Wang et al., 2003; Peñaflor et al., 2007). However, based on an analysis of the eddy-induced curls calculated from altimetry-derived geostrophic currents, we found poor correlation between the Chl-*a* concentration and eddy-induced curls (not shown).

Conclusions

The present study revealed the spatial distribution and interannual variation of the winter phytoplankton bloom northwest of Luzon. The concentration of the winter high Chl-*a* patch was significantly correlated with EPV, EV, SP $Temp_{75}$ and MLD. It was thought that the wind-induced upwelling (Ekman pumping) and the entrainment associated with the surface wind stirring and heat loss may play important roles in the high winter Chl-*a* blooms. The EV, EPV, SP may be good indicators of the uptake of nutrients available to phytoplankton in eutrophic layers; while the $Temp_{75}$ and MLD may merely represent the degree of the intrusion of the warm Kuroshio water.

Acknowledgements

This work was supported by the National Key Basic Research Program of China (2011CB403504), National Natural Science Foundation of China (project number 41006070), and the Canadian Space Agency Government Related Initiative Program. Helpful comments were received from two anonymous reviewers.

References

Behrenfeld, M.J., Falkowski, P.G., 1997. Photosynthetic rates derived from satellite-based chlorophyll concentration. Limnol. Oceanogr. 42(1), 1–20.

Behrenfeld, M.J., O'Malley, R.T., Siegel, D.A., McClain, C.R., Sarmiento, J.L., Feldman, G.C., Milligan, A.J., Falkowski, P.G., Letelier, R.M., Boss, E.S., 2006. Climate-driven trends in contemporary ocean productivity. Nature 444, 752–755.

Boyer, T.P., Antonov, J.I., Garcia, H.E., Johnson, D.R., Locarnini, R.A., Mishonov, A.V., Pitcher, M.T., Baranova, O.K., Smolyar, I.V., 2006. *NOAA Atlas NESDIS 60*. U.S. Government Printing Office, Washington, D.C.

Chao, S.-Y., Shaw, P.-T., Wu, S.-Y., 1996. Deep water ventilation in the South China Sea. Deep-Sea Res. I. 43(4), 445–466.

Chen, C.-C., Shiah, F.-K., Chung, S.-W., Liu K.-K., 2006. Winter phytoplankton blooms in the shallow mixed layer of the South China Sea enhanced by upwelling. J. Mar. Syst. 59, 97–110.

Fang, G., Fang, W., Fang, Y., Wang, K., 1998. A survey of studies on the South China Sea upper ocean circulation. Acta Oceanographica Taiwanica 37(1), 1–16.

Farris, A., Wimbush, M., 1996. Wind-induced Kuroshio intrusion into the South China Sea. J. Oceanogr. 52(6), 771–784.

Gong, G.-C., Liu, K.-K., Liu, C.-T., Pai, S.-C., 1992. The chemical hydrography of the South China Sea west of Luzon and a comparison with the west Philippine Sea, Terrestrial Atmospheric and Oceanic Sciences 3, 587–602.

Han, G. and Huang, W., 2009. Low-frequency sea level variability in the South China Sea and its relationship with ENSO. Theoretical and Applied Climatology 97, 41–52.

Hu, J., Kawamura, H., Hong, H., Qi, Y., 2000. A review on the currents in the South China Sea: Seasonal circulation, South China Sea warm current and a southwestward current and Kuroshio intrusion. J. Oceanogr. 56, 607–624.

Lalli, C.M., Parsons, T.R., 1997. *Biological Oceanography: An Introduction. 2nd Ed.* Pergamon Press, Oxford.

Li, L., Nowlin, W.D., Su, J.L., 1998. Anticyclonic rings from the Kuroshio in the South China Sea. Deep-Sea Res. I, 45(9), 1469–1482.

Liu, K.-K., Chao, S.-Y., Shaw, P.T., Gong, G.-C., Chen, C.-C., Tang, T.Y., 2002. Monsoon-forced chlorophyll distribution and primary production in the South China Sea: observations and a numerical study. Deep Sea Res., Part I, 49, 1387– 1412.

Liu, W.T., Tang, W., 1996. Equivalent neutral wind. JPL Publication, Vol. 96–17. Available at http://airsea-www.jpl.nasa.gov/data/data.html

Martin, J.H., Knauer, G.A., Karl, Knauer, DM., Broenkow, Karl, W.W., 1987. Vertex: carbon cycling in the northeast Pacific. Deep-Sea Res. 34, 267–286.

Mendoza, V.M., Villanueva, E.E., Adem, J., 2005. On the annual cycle of the sea surface temperature and the mixed. Atmõsfera 18 (2), 127–148.

Morton, B., Blackmore, G., 2001. South China Sea, Mar. Pollut. Bull. 42(12),1236–1263.

Olivieri, E.T., 1983. Colonization, adaptations and temporal changes in diversity and biomass of a phytoplankton community in upwelled water off the Cape Peninsula, South Africa, in December 1979, S. Afr. J. Mar. Sci. l.(1), 77–109.

Pan, Y, Tang, D.L., Weng, D.H., 2010. Evaluation of the SeaWiFS and MODIS chlorophyll-*a* algorithms used for the North South China sea during the summer season. Terr. Atmos. Oceean. Sci., 20(6), 997–1005, doi: 10.3319/TAO.2010.02.11.01(Oc).

Peñaflor, E.L., Villanoy, C.L., Liu, C.T., David, L.T., 2007. Detection of monsoonal phytoplankton blooms in Luzon Strait with MODIS data. Remote Sensing of Environment, doi:10.1016/j.rse.2007.01.019.

Qu, T., 2000. Upper-layer circulation in the South China Sea. J. Phys. Oceanogr. 30, 1450–1460.

Shaw, P.-T., 1991. The seasonal variation of the intrusion of the Philippine Sea into the South China Sea. J. Geophys. Res. 96, 821–827.

Shaw, P.-T., Chao, S.-Y., Liu, K.-K., Pai, S.-C., Liu, C.-T., 1996. Winter upwelling off Luzon in the northeastern South China Sea. J. Geophys Res. 101(C7), 16435–16488.

Sverdrup, H.U., Johnson, M.W., Fleming, R.H., 1946. The Oceans: Their physics, chemistry and general biology. Prentice Hall Inc., New York.

Tang, D.L., Ni, I.H., Kester, D.R., Müller-Karger, F.E., 1999. Remote sensing observations of winter phytoplankton blooms southwest of the Luzon Strait in the South China Sea. Mar. Ecol. Prog. Ser. 191, 43–51.

Udarbe-Walker, M.J.B., Villanoy, C.L., 2001. Structure of potential upwelling areas in the Philippines. Deep-Sea Research I 48, 1499–1518.

Wang, G.H., Su, J.L., Chu, P.C., 2003. Mesoscale eddies in the South China Sea observed with altimeter data. Geophys. Res. Lett., 30(21), doi:10.1029/2003GL018532

Zhao, H., Tang, D.L., 2007. Effect of 1998 El Niño on the distribution of phytoplankton in the South China Sea, J. Geophys. Res., 112, C02017, doi:10.1029/2006JC003536.

Zheng, Z.-W., Ho, C.-R., Kuo, N.-J., 2007. Mechanism of weakening of west Luzon eddy during La Niña years, Geophys. Res. Lett., 34, L11604, doi:10.1029/2007GL030058.